# Topological Analysis of Electron Density Distribution Taken from a Pseudopotential Calculation

**SERGEI F. VYBOISHCHIKOV, ANIBAL SIERRAALTA, and GERNOT FRENKING***

*Fachbereich Chemie der Philipps–Universität Marburg, Hans-Meerwein-Strasse, D-35032 Marburg, Germany*

*Received 8 March 1996; accepted 20 April 1996*

**ABSTRACT**

Theoretical studies of the electron density topology at the bond critical point for some small molecules, Ti, and Mo organometallic complexes were undertaken in order to understand the reason for the failure of the topological analysis of the coreless electron densities obtained from a pseudopotential calculation. We show that the absence of the core electron density is the main reason for such behavior. The erratic behavior of the effective core potentials electron densities can be corrected by adding atomic electron core density obtained from a single-atom Hartree–Fock calculation. The effect of orthogonalization of the core orbital with the valence orbitals was also investigated. © 1997 by John Wiley & Sons, Inc.

## Introduction

The pseudopotential approach has become an important and conventional tool for calculating heavy-element compounds such as transition metal complexes. In recent years the effective core potentials (ECPs) have been used intensively by the quantum chemical community to calculate and predict molecular geometries as well as other molecular properties.[1] Central to the concept of pseudopotentials is the idea that the core electrons of an atom are chemically inactive and can be substituted by some effective potentials instead of being treated explicitly. Furthermore, relativistic effects that are important for heavy elements[2] can be incorporated into the pseudopotentials. This leads to the well-known relativistic or quasirelativistic ECPs (RECPs), which have a relativistically derived core potential and a nonrelativistic valence Hamiltonian. The ECPs are analytically expanded in terms of Gaussian-type radial functions. These ECPs produce nodeless or low-node atomic pseudoorbitals that are smoothed out in the core region. Parallel to the development of the ECPs, ab initio model potentials[3] were proposed. In the

*Author to whom all correspondence should be addressed.



CCC 0192-8651 / 97 / 030416-14

latter approach, the pseudoorbitals retain the correct nodal structure. However, less computational cost of the model potentials in comparison with the ECPs made the ECP ansatz the most widely used in the quantum chemistry area.

The theory atoms in molecules (AIM) developed by Bader[4] is based on the analysis of the one-electron spinless density function $\rho(\mathbf{r})$. An important role in the topological theory is attributed to the critical points of the molecular electronic density, i.e., points where the gradient of $\rho(\mathbf{r})$ vanishes ($\nabla\rho = 0$). For the classification of critical points the pair $(r, \sigma)$ is used, where $r$ and $\sigma$ are rank and signature of the Hessian matrix $[\partial^2\rho/\partial x_i\,\partial x_j]$, respectively. Critical points of a $(3, -3)$ type (maxima) coincide with nuclear positions (although nonnuclear maxima are also known[5]; $(3, -1)$ points are located between nuclei of chemically linked atoms and therefore they are called bond critical points. To classify the different chemical bonds, the sign of either the Laplacian of the electron density $\nabla^2\rho$ or the electronic energy density $H$ at the bond critical point $\mathbf{r}_c$ were proposed.[6,7]

However, the applicability of the topological analysis of the electron density distribution to densities obtained from quantum chemical calculations, using the relativistic or nonrelativistic ECP approach, remains unclear. In many cases it was employed successfully,[8] but failures were also reported.[9] The different results of the topological analysis of all-electron (AE) densities were discussed by Sierraalta and Ruette[9] and briefly mentioned by Bo et al.[10] Therefore, it is important not only to clarify and understand why in some cases the topological analysis of the ECP electron densities fails, but also to indicate whether the failures can be overcome. One principal difficulty lies in the fact that pseudopotential calculations yield only densities, which do not include the core electrons. In the areas close to the nuclei, such coreless densities behave in a different manner than the AE density does. For example, the electron density $\rho(\mathbf{r})$ using RECP/ECP wave functions does not have maxima at nuclear positions. Even though core electrons are not important in the formation of chemical bonds, the ECP approach sometimes gives an incorrect density distribution, and no $(3, -1)$ critical point in $\rho$ between chemically linked atoms can be found.[9] The aim of the present work was to investigate in which cases the topological analysis of the coreless density that comes from an ECP calculation is applicable and whether it can be corrected. We analyze the properties at the bond critical point $\mathbf{r}_c$ obtained from AE calculations and those obtained using pseudopotentials for several small molecules as well as for some transition metal complexes.

## Theoretical Procedure

### CALCULATIONS

Ab initio quantum chemical calculations were carried out to obtain the necessary electron densities. Geometry optimizations were done using the restricted closed-shell Hartree–Fock method employing ECPs. For nonmetal atoms, the quasirelativistic pseudopotentials of the Stuttgart group[11] were used. The original basis sets were augmented with one polarization $d$ function, while the most diffuse $p$ functions for halogen atoms were not used. This results in (31/31/1) valence basis sets. For the geometry optimizations of the molybdenum and titanium complexes, we used the small-core ECP of Hay and Wadt,[12] in which the $(n-1)$ $s^2$, $(n-1)$ $p^6$, $(n-1)$ $d^m$, and $ns^q$ electrons are treated explicitly. The original (5/5/4) basis of the Mo atom was modified according to Jonas et al.[13] to yield a (441/2111/31) basis set. For titanium, a (441/2111/41) contraction of the original (5/5/5) basis set was employed. To study the effect of the outer-shell core electrons upon the AIM calculations, we also carried out calculations using the Hay–Wadt large-core ECPs,[14] in which only the $(n-1)$ $d^m$ and $ns^q$ electrons are used at geometries obtained with the small-core ECPs. For AE calculations of second-row atoms Krishnan et al.[15] 6–311$G^{**}$ basis sets were used, while for third-row atoms MacLean–Chandler's[16] (631111/42111/1) basis sets were employed. For AE calculations of molecules containing iodine, bromine, molybdenum, and titanium atoms, Andzelm et al.'s basis sets[17] were employed. With the geometries obtained from optimizations using pseudopotentials, single-point AE Hartree–Fock calculations were performed. The calculated geometries used in this work are reported in Table I. All calculations were done with the Gaussian 92 program package[18] on a Silicon Graphics Power Challenge computer.

The topological analysis of $\rho(\mathbf{r})$ was carried out with the EXTREME program.[19] Atomic charges were determined by a locally modified version of PROAIM.[20,21] In addition, the bond orders were calculated using the approach developed by Ángyán et al.[22] It was shown that these bond

**TABLE I.**
**Calculated Molecular Geometries.**

| Molecule | Parameter | Value (Å, degrees) |
|---|---|---|
| $Cl_2$ | R (Cl—Cl) | 2.013 |
| $Br_2$ | R (Br—Br) | 2.318 |
| $I_2$ | R (I—I) | 2.696 |
| BrCl | R (Br—Cl) | 2.151 |
| BrI | R (Br—I) | 2.487 |
| LiBr | R (Li—Br) | 2.146 |
| SiO | R (Si—O) | 1.485 |
| $SH_2$ | R (S—H) | 1.324 |
| | ∠(H—S—H) | 94.6 |
| $SF_6$ | R (S—F) | 2.183 |
| $CH_3$—$SiH_3$ | R (C—Si) | 1.882 |
| | R (H—C) | 1.085 |
| | R (Si—H) | 1.477 |
| | ∠(H—C—Si) | 111.1 |
| | ∠(H—Si—C) | 110.5 |
| $P_2$ | R (P—P) | 1.877 |
| $As_2$ | R (As—As) | 2.105 |
| $PCl_3$ | R (P—Cl) | 2.078 |
| | ∠(Cl—P—Cl) | 100.1 |
| $PH_3$ | R (P—H) | 1.418 |
| | ∠(H—P—H) | 94.8 |
| $(CO)_5Mo(CH_2)$ | R(Mo—$CH_2$) | 2.089 |
| | R(Mo—CO *cis*) | 2.098 |
| | R (Mo—CO *trans*) | 2.196 |
| $TiF_4$ | R (Ti—F) | 1.744 |

orders have virtually the same values as those by Cioslowski and Mixon,[23] but they can be computed in a simpler way. The electron kinetic energies of the atoms using Bader's definition of atoms in molecules[4] were calculated.

## CORE DENSITY

The erratic behavior of the ECP electronic density appears to be the main reason for the difficulties encountered in the topological analysis of such densities (vide supra). One possibility of solving this problem lies in the addition of single-atom AE core density $\rho_{CORE}(\mathbf{r})$ to the coreless density $\rho_{ECP}(\mathbf{r})$ obtained in a pseudopotential calculation: $\rho_{NEW}(\mathbf{r}) = \rho_{ECP}(\mathbf{r}) + \rho_{CORE}(\mathbf{r})$. To obtain the core density, we calculated the totally symmetric $S$ state of the neutral atom or the corresponding ion with the restricted closed- or open-shell AE Hartree–Fock method using the same basis sets as in the molecular single-point calculation. Thus, the core densities of the chlorine, sulfur, and phosphorus atoms were obtained calculating the $^1S$ state of the $Cl^-$ anion, and the $^4S$ state of the $S^+$ cation, and of neutral P, respectively. Alternatively, ground states of the cations corresponding to the ECP core can be used instead. In principle, it would be better to use the core density obtained by numerically solving the atomic Hartree–Fock or Dirac–Fock equation, because they are used to fit pseudopotentials. However, sufficiently large Gaussian bases, as used in this work, should reproduce the core density well and require much less computational effort. One should be aware, however, that the difference between $\rho_{NEW}$ and $\rho_{AE}$ is in part accounted for by the fact that the nonrelativistic core was added to the valence density obtained using a quasirelativistic ECP.

## ORTHOGONALIZED CORE DENSITY

The simple addition of atomic core density to molecular coreless density from an ECP calculation appears to be a suitable approach for approximating AE densities as long as $\rho(\mathbf{r})$ or quantities derived thereof are of interest. Although Bader's topological theory requires only the one-electron density, some approaches based on it need orbitals as well. On the other hand, one might encounter difficulties if the attached atomic core orbitals are not orthogonal to the valence molecular orbitals. It is known that core electrons are mainly concentrated in the vicinity of the nucleus, while the valence electrons are further away from it. Therefore, the core orbitals should be nearly orthogonal to the molecular valence orbitals. Exact orthogonality is reached, however, only for single-atom orbitals provided that ab initio model potentials[3] are used. In the case of nodeless ECPs, orthogonality no longer holds. The overlap between molecular valence and attached atomic core orbitals cannot be neglected because it leads to the violation of some important properties of the density matrix **D**, constructed from such orbitals, such as idempotency (**DSD** = **D**, where S is the overlap matrix; this is only true for the Hartree–Fock density matrix) and trace (tr **DS** = number of electrons). In addition, if the molecule contains several atoms for which pseudopotentials are applied, the core orbitals belonging to these atoms are also not orthogonal. However, the overlap between different cores is small if the nuclear separation is large enough. This assumption is essential for the functionality of the ECPs.[12] Because the molecular valence orbitals are orthonormal, only core orbitals need to be

orthogonalized with each other and with molecular valence orbitals. Using orthogonalized orbitals, we obtain the corrected electron density $\rho_{ORT}$.

The choice of the orthogonalization procedure does not play a role at the Hartree–Fock level. Indeed, two different orthogonalizations are identical up to a unitary transformation. Because a unitary transformation of molecular orbitals $\varphi_i$ does not change the Slater determinant, all density matrices, including the one-electron density $\rho$ corresponding to the Slater determinant, remain unaltered. This does not hold true for a correlated wave function whose density is expressed via a weighted sum over natural orbitals $\chi_i$, with the occupation numbers $n_i$ being weighting factors. An arbitrary orthogonalization of valence natural and canonical core orbitals would mix the two sets of orbitals, and one encounters the problem of determining new occupation numbers $\tilde{n}_i$, which would correspond to orthogonalized natural orbitals $\tilde{\chi}_i$. To avoid this difficulty, one can use an orthogonalization procedure that keeps natural valence orbitals unchanged: $\tilde{\chi}_i = \chi_i$; $\tilde{n}_i = n_i$. This is possible because $\chi_i$ are initially orthogonal to each other. Therefore, one can apply the operator $\hat{P} = 1 - \sum_i |\chi_i\rangle\langle\chi_i|$, where the summation runs initially over all valence orbitals. At further orthogonalization steps, the summation runs over the previously orthogonalized orbitals. $\hat{P}$ projects an orbital onto the orthogonal complement of set $\{\chi_i\}$. This technique is equivalent to the Gram–Schmidt orthogonalization. A disadvantage of this approach is that the resulting set of orthogonalized orbitals depends on the sequence of orthogonalization. The orbitals that are last involved in the orthogonalization procedure are changed more. As a result, the nodal structure of the orbitals is very different in comparison with that of the orbitals obtained from AE calculation. First, core orbitals (even $1s$) orthogonalized to molecular valence orbitals contain more nodes than given by the principal quantum number of the respective atom, whereas valence orbitals have less nodes because they are obtained using nodeless ECPs. Second, if there are several symmetrically equivalent atoms at which ECPs are applied, the orthogonalized core orbitals possess different numbers of nodes and do not transform as an irreducible representation of the molecular point group. However, the total density remains totally symmetric. In the present work, the orthogonalization of the orbitals was performed using a program developed by the authors.

## Results and Discussion

As mentioned above, one of the principal disadvantages of $\rho_{ECP}(\mathbf{r})$ is the absence of the contribution of the core electron density. Figure 1 shows the difference between the AE density and ECP derived electron density using the 10-electron MWB pseudopotential[11] for the phosphorus atom. As expected, the AE density $\rho_{AE}$ exhibits a very distinct maximum at the nucleus. Conversely, the ECP density $\rho_{ECP}$ displays a smoothed local minimum at the nucleus. The densities $\rho_{ECP}$ and $\rho_{AE}$ behave differently up to $r \sim 1.5$ au, and this area penetrates deeply into the chemically interesting region. For larger $r$, $\rho_{ECP}$ and $\rho_{AE}$ are very close. For instance, at $r = 2$ au, the difference is only 0.26%. $\rho_{ECP}(r)$ has a maximum at $r = 1.22$ au. In 3-dimensional (3-D) space this corresponds to a continuum of degenerate $(1, -1)$ critical points. A perturbation such as the presence of another atom eliminates the degeneracy and results in a set of $(3, -1)$ and $(3, -3)$ critical points. Thus, in a molecule there would be an unpredictable number of such critical points close to the nucleus. Within the framework of the topological analysis one is usually interested in the behavior of $\rho$ in the internuclear region only. Therefore, in principle, the spurious topology of $\rho_{ECP}$ in the nuclear region does not necessarily affect the results. We want to point out, however, that the existence of the appropriate $(3, -1)$ critical point in $\rho_{ECP}$ between chemically bound atoms depends on whether the expected critical point belongs to the ascending or descending part of $\rho_{ECP}(r)$ shown in Figure 1.

Let us now consider $\rho_{NEW}$ obtained by the addition of AE core density to $\rho_{ECP}$ in the phosphorus atom. The corresponding curve on Figure 1 lies very close to the AE density curve with the exception of a small area at $r \sim 1$ au, where the difference can be as much as 9%. At $r = 1.5$ au, the difference is only 1% and diminishes rapidly with increasing $r$. Thus, a significant improvement is achieved by using $\rho_{NEW}$ instead of $\rho_{ECP}$. The addition of density of core orbitals orthogonalized to ECP valence orbitals gives $\rho_{ORT}(r)$, which behaves qualitatively like $\rho_{AE}(r)$ or $\rho_{NEW}(r)$. In the area close to the nucleus, $\rho$ is significantly improved by the orthogonalization (Fig. 1). At $r = 0.5$ au, the difference between $\rho_{AE}$ and $\rho_{ORT}$ is only 0.03%, while the difference between $\rho_{AE}$ and $\rho_{NEW}$ is 0.5%. However, $\rho_{ORT}$ is smaller than $\rho_{AE}$ be-

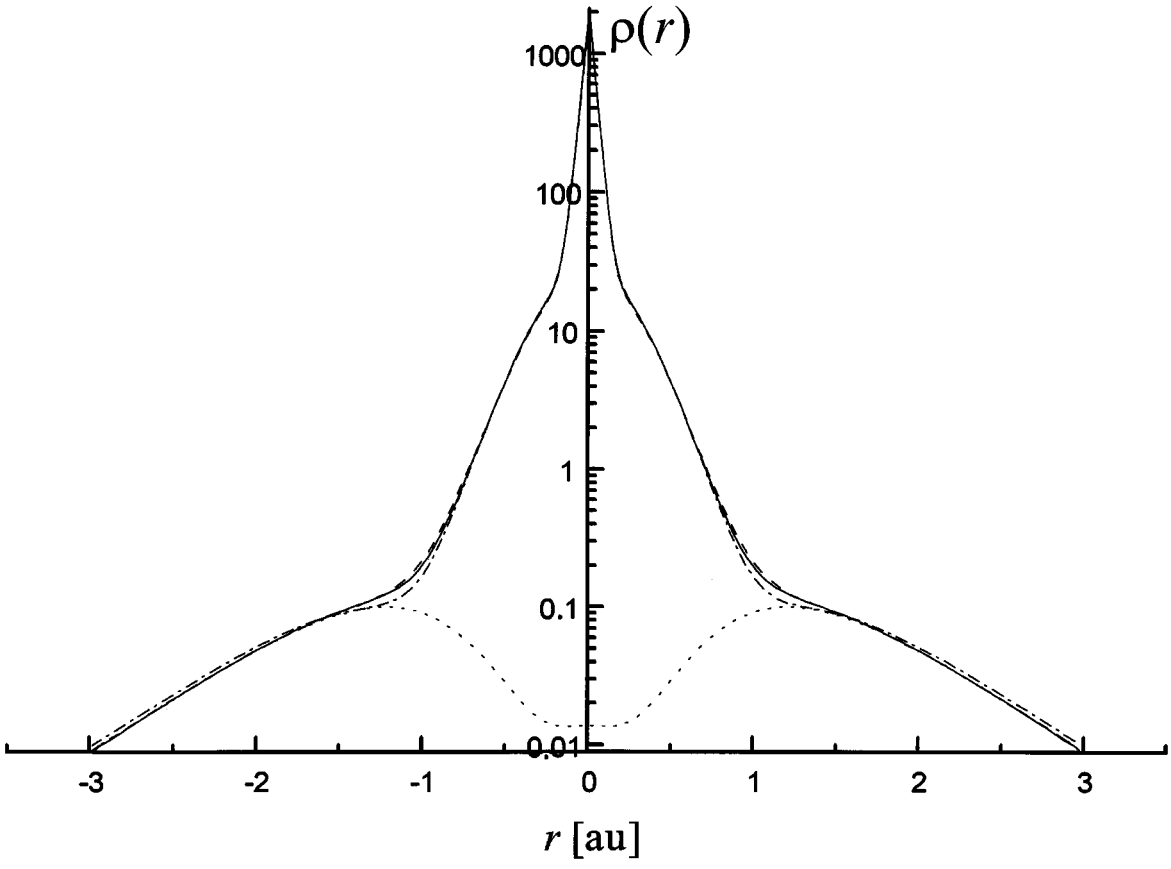


**FIGURE 1.** Plot of the electron density versus the distance from the nucleus for the phosphorus atom. (—) All-electron density ( $\rho_{AE}$), (- - -) the density obtained from the pseudopotential calculation ( $\rho_{ECP}$), (– – –) the density obtained by addition of the core density to the pseudopotential density ( $\rho_{NEW}$), (–·–·–) the density obtained by addition of the orthogonalized core density to the pseudopotential density ( $\rho_{ORT}$).

tween $r = 0.54$ and 1.6 au, the difference being up to 20%. At greater, $r$, $\rho_{ORT}$ becomes larger than $\rho_{AE}$, $\rho_{ECP}$, and $\rho_{NEW}$. It follows that $\rho_{ORT}$ yields an improvement over $\rho_{NEW}$ in the core region, while in the valence area the performance of $\rho_{ORT}$ is worse than $\rho_{NEW}$. The reasons for this behavior of $\rho_{ORT}$ can be understood using a lithium atom as an example (see Fig. 2). After orthogonalization of the 1*s* orbital to the nodeless 2*s*-valence orbital, the 1*s*-core orbital acquires a node and becomes much more diffuse in order to provide sufficient negative overlap with the 2*s* orbitals. This shows that the orthogonalization process produces new core orbitals that are more diffuse than the original ones and possess a higher number of nodes as shown in Figure 2.

Table II shows the properties of the electronic density at the bond critical point for some molecules. For $PL_3$ (L=Cl, H) one does not find a (3, −1) critical point in $\rho_{ECP}$ between the phosphorus atom and the ligands. The topology of $\rho_{ECP}$ does not reflect the bonding situation in the two molecules. For example, in $PH_3$ there are bond critical points between the hydrogen atoms, and the corresponding bond paths are very curved. Such a situation has no physical meaning, because there are no chemical bonds between the H atoms. The AE density $\rho_{AE}$ for $PL_3$, on the other hand, has three (3, −1) critical points corresponding to P—L bonds and no critical points between the H or Cl atoms, which is in agreement with the bonding pattern. Figure 3a displays the electron density distribution in logarithmic scale for the $PCl_3$ molecule. For all AE density $\rho_{AE}$ between phosphorus and chlorine, we obtain a pattern typical for two atoms connected by a chemical bond. It contains two sharp maxima located at the nuclei and a saddle point that corresponds to the (3, −1) bond critical point in the 3-D $\rho_{AE}$ distribution. The density $\rho_{ECP}$ obtained from the wave function calculated using pseudopotentials on both phosphorus and chlorine atoms is completely different.

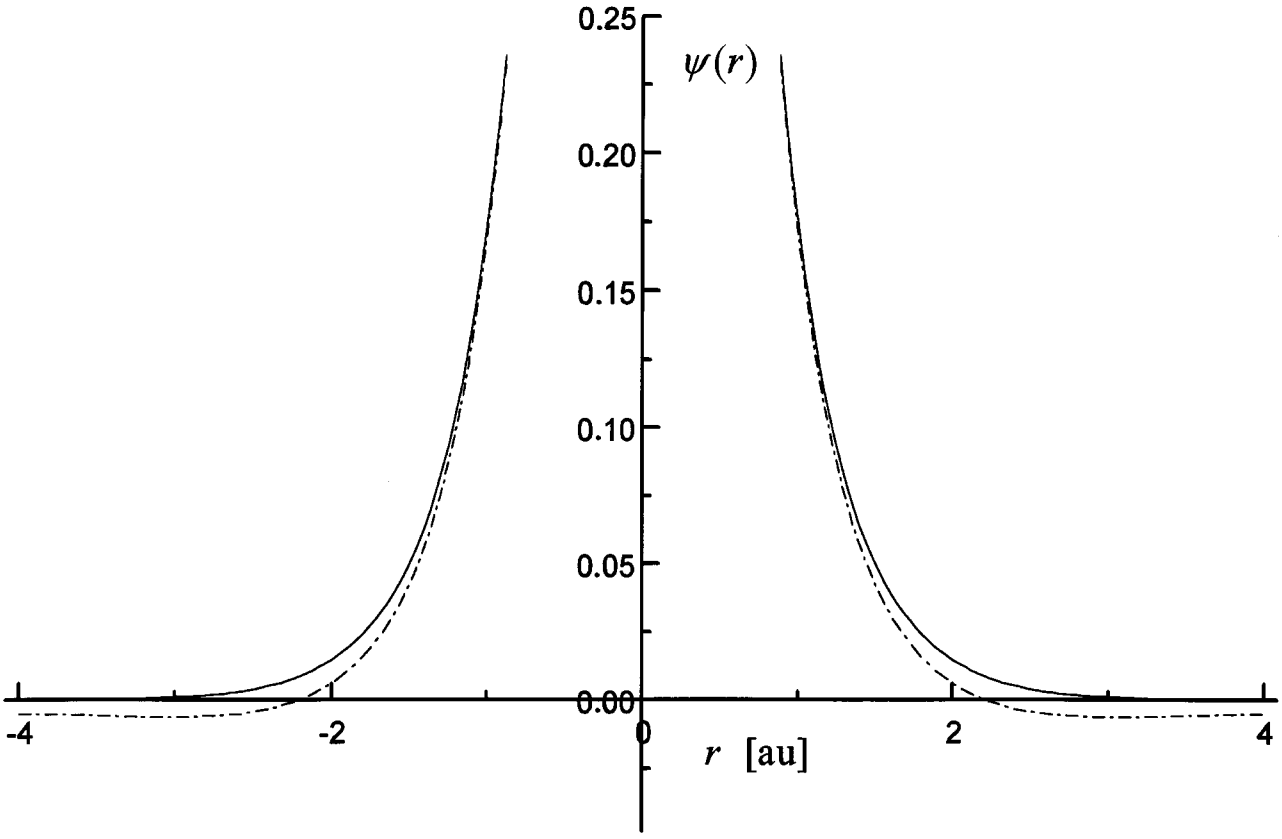


**FIGURE 2.** Plot of the 1*s* orbital of lithium atom. (—) The original orbital obtained from an ROHF calculation, (–-–-) the 1*s* orbital orthogonalized to the 2*s* orbital obtained from an ECP calculation.

Similar to the density of an isolated phosphorus atom, $\rho_{ECP}$ possesses local minima at the nuclear positions. However, a maximum in the neighborhood of the phosphorus atom does not exist. On the other hand, $\rho_{ECP}$ presents a maximum at a distance of 1.05 au from the Cl atom and decreases monotonically from this maximum to the phosphorus nucleus. There is no $(3, -1)$ critical point between the P and Cl atom. This is not due to a principal failure of the pseudopotential approach or to its unsuitability for this particular molecule. Indeed, within a quite large area in the internuclear region $\rho_{ECP}$ reproduces the AE density $\rho_{AE}$ quite well. For example, in an 1-au long interval in the middle of the P—Cl bond the density $\rho_{ECP}$ differs from $\rho_{AE}$ by at most 1%. Molecular orbital analysis shows that the same type and number of bonding and nonbonding orbitals in the valence space of $PCl_3$ are found in the AE case as in the ECP calculation. Therefore, it is reasonable to suppose that the lack of core density gives rise to the absence of the bond critical point.

The failure of the ECP density to reproduce the P—L bond critical points can be corrected by adding atomic core density to $\rho_{ECP}$. Figure 3a shows that the shape of $\rho_{NEW}$ and $\rho_{ORT}$ is qualitatively identical to $\rho_{AE}$. Sharp maxima at the nuclei are separated by a $(3, -1)$ critical point. $\rho_{NEW}$ and $\rho_{ORT}$ are quite close to $\rho_{AE}$ except for a small interval, where the difference is up to 10%. Unfortunately, this is in the area where the bond critical point is found. The values of $\rho(\mathbf{r}_c)$, $-H(\mathbf{r}_c)$, and $\nabla^2\rho(\mathbf{r}_c)$ for $PL_3$ (L=Cl, H) are underestimated in the case of $\rho_{NEW}$ compared to the $\rho_{AE}$ values. Thus, the properties of the critical points of $\rho_{AE}$, $\rho_{NEW}$, and $\rho_{ORT}$ differ significantly (see Table II). Orthogonalization of the core orbitals deteriorates the results. $\nabla^2\rho$ is especially affected; it has the wrong sign and its absolute value is overestimated. The bond critical point of the P—L bond is shifted toward the P atom. This displacement causes the net charge on the P atom calculated from $\rho_{NEW}$ to be highly positive.

For the calculation of the silicon-containing molecules (methylsilane and silicon monoxide), an ECP was applied only to the silicon atom. In both

**TABLE II.**
**Properties of Electron Density Critical Points in Phosphorus and Silicon Compounds.**

| Molecule A—B Bond | Method | $\rho(\mathbf{r}_c)$ ($e \cdot au^{-3}$) | $\nabla^2\rho(\mathbf{r}_c)$ ($e \cdot au^{-5}$) | $H(\mathbf{r}_c)$ hartree · $au^{-3}$) | $\varepsilon$ | $\mathbf{R}_{A\text{-}CP}$ (au) | Net Charge on **A** | Bond Order | $K(\mathbf{A})$ / $K(\mathbf{A})_{AE}$ |
|---|---|---|---|---|---|---|---|---|---|
| $PCl_3$ | | | | | | | | | |
| P—Cl | AE | 0.128 | −0.214 | −0.112 | 0.106 | 1.502 | 1.577 | 0.892 | 1.000 |
| P—Cl | NEW | 0.117 | −0.027 | −0.080 | 0.163 | 1.438 | 1.828 | 0.840 | 0.984 |
| P—Cl | ECP | | | | No (3, −1) bond critical point found | | | | |
| P—Cl | ORT | 0.114 | 0.179 | −0.088 | 0.263 | 1.315 | 2.168 | 0.732 | 0.994 |
| $PH_3$ | | | | | | | | | |
| P—H | AE | 0.159 | −0.067 | −0.158 | 0.127 | 1.300 | 1.590 | 0.857 | 1.000 |
| P—H | NEW | 0.151 | −0.016 | −0.112 | 0.128 | 1.346 | 1.515 | 0.891 | 0.984 |
| P—H | ECP | | | | No (3, −1) bond critical point found | | | | |
| P—H | ORT | 0.140 | 0.398 | −0.107 | 0.169 | 1.243 | 2.085 | 0.747 | 0.995 |
| SiO | | | | | | | | | |
| Si—O | AE | 0.196 | 2.003 | −0.060 | 0.000 | 1.172 | 1.525 | 1.238 | 1.000 |
| Si—O | NEW | 0.201 | 1.835 | −0.016 | 0.000 | 1.195 | 1.529 | 1.284 | 0.988 |
| Si—O | ECP | | | | No (3, −1) bond critical point found | | | | |
| Si—O | ORT | 0.177 | 2.269 | −0.013 | 0.000 | 1.172 | 1.636 | 1.109 | 0.996 |
| $CH_3$—$SiH_3$ | | | | | | | | | |
| C—Si | AE | 0.120 | 0.286 | −0.073 | 0.000 | 2.214 | −0.786 | 0.456 | 1.000 |
| C—Si | NEW | 0.121 | 0.257 | −0.056 | 0.000 | 2.187 | −0.778 | 0.494 | 1.000 |
| C—Si | ECP | | | | No (3, −1) bond critical point found | | | | |
| C—Si | ORT | 0.110 | 0.502 | −0.050 | 0.000 | 2.239 | −0.863 | 0.346 | 1.002 |
| Si—H | AE | 0.118 | 0.213 | −0.075 | 0.005 | 1.356 | 2.903 | 0.472 | 1.000 |
| Si—H | NEW | 0.119 | 0.183 | −0.061 | 0.007 | 1.382 | 2.858 | 0.510 | 0.989 |
| Si—H | ECP | | | | No (3, −1) bond critical point found | | | | |
| Si—H | ORT | 0.109 | 0.421 | −0.055 | 0.008 | 1.326 | 3.247 | 0.353 | 0.996 |

$\varepsilon$ is the ellipticity of the critical point; $\varepsilon = \min\{\lambda_1, \lambda_2\} / \max\{\lambda_1, \lambda_2\} - 1$ where $\lambda_1$ and $\lambda_2$ are the negative eigenvalues of the Hessian matrix.[24]

$R_{A\text{-}CP}$ is the distance between atom *A* and the (3, −1) critical point.

$CH_3SiH_3$ and SiO, no bond critical points (3, −1) were found between Si and the chemically bound atoms. As shown in Figure 3b, the AE density distribution $\rho_{AE}$ between the carbon and silicon atoms in $CH_3SiH_3$ has sharp maxima at the nuclei separated by a well-defined (3, −1) critical point. The density $\rho_{ECP}$ agrees excellently with $\rho_{AE}$ everywhere, except for an area around the Si nucleus. At a distance of 1.8 au from the Si atom, $\rho_{AE}$ and $\rho_{ECP}$ differ by 1.5%, and this difference decreases rapidly as the distance increases. At smaller distances, however, $\rho_{AE}$ and $\rho_{ECP}$ diverge significantly. Thus, $\rho_{ECP}$ decreases monotonically from the carbon nucleus to silicon and displays a minimum at the Si nucleus. Therefore, no critical point is found between the chemically bound Si and C atoms. We see again that despite the fact that the pseudopotential approach works properly, $\rho_{ECP}$ has the wrong topology and cannot be used for the topological analysis. As in all cases studied here, the addition of atomic core density recovers the correct behavior of the electron density with maxima at nuclear positions and (3, −1) critical points in the bond region. $\rho_{NEW}$ exhibits the correct behavior and is in general close to $\rho_{AE}$ · $\rho_{NEW}$ also provides an improvement in some areas where $\rho_{ECP}$ is already in reasonable agreement with $\rho_{AE}$. For example, at 1.8 au from the Si atom, the difference between $\rho_{AE}$ and $\rho_{NEW}$ is only 1%. However, there are also areas where $\rho_{NEW}$ overestimates the density given by $\rho_{AE}$. The density $\rho_{ORT}$ obtained from the orthogonalized core orbitals behaves qualitatively as $\rho_{AE}$ and $\rho_{NEW}$. In some regions, $\rho_{ORT}$ overestimates $\rho_{AE}$ and underestimates it in others. The largest difference between $\rho_{AE}$ and $\rho_{ORT}$ is 10.3%, and this occurs in the crucially important region where both functions have critical points. In this area $\rho_{NEW}$ deviates from $\rho_{AE}$ at most by 6.6%. Therefore, orthogonalization of core orbitals does not necessarily provide an improvement of the electron density distribution.

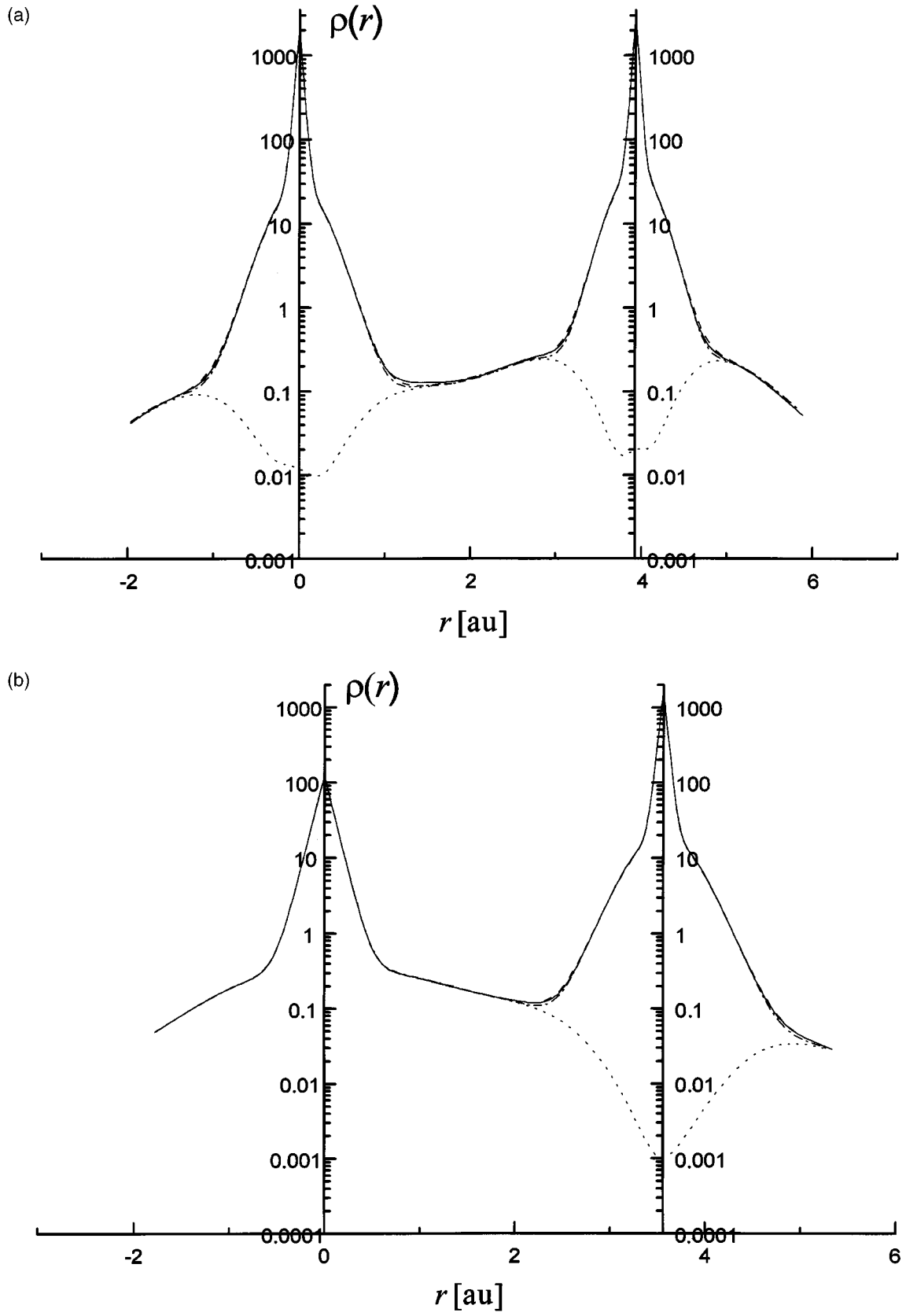


**FIGURE 3.** Plot of the electron density distribution along the chemical bond in (a) $PCl_3$ and (b) $CH_3SiH_3$. Notations are the same as in Figure 1.

Table II shows that the calculated value for the electron densities $\rho_{NEW}$ and $\rho_{ORT}$ and their associated Laplacians $\nabla^2\rho_{NEW}$ and $\nabla^2\rho_{ORT}$ at the Si—C and Si—H bond critical points are in reasonable agreement with the AE values. However, $-H(\mathbf{r}_c)$ is too low when $\rho_{NEW}$ and $\rho_{ORT}$ are used. $\rho_{NEW}$ gives better values than $\rho_{ORT}$ for the bond orders. For the C—H bond all four methods yield almost identical results, because the pseudopotential on the silicon atom renders only minute effects on the density far from it.

As discussed above, the orthogonalization process yields rather diffuse core orbitals. Because these orbitals belong to the atomic cores, their associated electron density is highly depleted in regions close to the bond critical point. This produces a large positive value of the total Laplacian of $\rho_{ORT}$ at this point. In addition to the local density properties at the (3, −1) critical point $\rho(\mathbf{r}_c)$, $\nabla^2\rho(\mathbf{r}_c)$, and $\varepsilon(\mathbf{r}_c)$, atomic integral properties such as the net charge and the total kinetic energy $K$ of the atom **A** were calculated within the framework of the topological theory

$$K(\mathbf{A}) = -\frac{1}{2}\sum_{i}^{NO} n_i \int_{\Omega_\mathbf{A}} \chi_i \nabla^2\chi_i \, dV.$$

Here $n_i$ are the occupation numbers and $\chi_i$ are the molecular canonical or natural orbitals. The ratio of $K(\mathbf{A})$ to the total kinetic energy $K(\mathbf{A})_{AE}$ of the same atom calculated with the AE wave function as well as bond orders are reported in Table II. The results indicate that reasonable values can be obtained for the net charges and bond orders using nonorthogonalized orbitals. Even though the values for the kinetic energy and the bond orders are reasonable, they are formally wrong because the equations for $K(\mathbf{A})$ and the bond orders were derived under the assumption of orthonormal molecular orbitals. On the other hand, better values for the $K(\mathbf{A})/K(\mathbf{A})_{AE}$ ratio are obtained within the orthogonalized-orbital scheme. The success of $\rho_{NEW}$ in comparison with $\rho_{ORT}$ is based on the fact that, in the $\rho_{NEW}$ approach, the core electron density is better represented than in the $\rho_{ORT}$ scheme where the overly diffuse core orbitals lead to undesirable results.

In Table III the topological properties of the electron density for a series of bromine compounds are reported. For these compounds, the ECP densities have a (3, −1) bond critical point between the nuclei. In BrCl there are two spurious weak maxima between the nuclei, which are 1.31 au from Br and 1.05 au from Cl. In 3-D space they are (3, −3) critical points. The magnitude of $\rho_{ECP}$ at the bond critical point is 87% of that in one of two maxima. The topology of $\rho_{ECP}$ distribution is incorrect, because the calculated local maxima have no physical meaning. The behavior of $\rho_{ECP}$ in the area of the bond critical point is similar to that of $\rho_{AE}$. The values of $\rho_{ECP}$ and $\rho_{AE}$ at the critical point are also quite close with a difference of only 3%. As shown in Table III, the properties of $\rho_{ECP}$ are close to those given by $\rho_{AE}$. Moreover, one can determine the zero-flux surfaces and then evaluate atomic charges as well as other atomic properties by employing $\rho_{ECP}$. Thus, the topological theory of molecular structure is applicable to an ECP density as long as (3, −1) critical points are found between chemically linked atoms. However, in this case the bond path is not well established because it terminates at the spurious density maxima rather than at the nuclei. In the chemically important area around the critical point, $\rho_{NEW}$ is less than $\rho_{AE}$ by at most 2.4%. $\rho_{ORT}$ is slightly larger than $\rho_{AE}$ in all areas except those closer to the nuclei, where the situation is reversed. In BrI the best agreement between AE and pseudopotential density is given by $\rho_{ORT}$. Interestingly, $\nabla^2\rho_{ECP}(\mathbf{r}_c)$ is negative, whereas the Laplacians obtained from other densities are positive. The energy density is also improved substantially by addition of core density, while the bond order is reproduced well if $\rho_{ECP}$ is used. For lithium bromide, which has a predominantly ionic bond, an ECP was applied only to the bromine atom. The results obtained by using $\rho_{ECP}$ are identical to AE values, and the use of corrected densities $\rho_{NEW}$ and $\rho_{ORT}$ does not change the results.

A quite different pattern emerges from the contour maps of the Laplacian of the electron densities for the BrCl molecule (Fig. 4). In the pseudopotential case, the space between the bonded atoms as well as the area surrounding the nuclei are characterized by negative values of $\nabla^2\rho$ instead of positive values as in the AE case. The difference is particularly pronounced for Br. The simple addition of core density drastically changes the shape of the Laplacian. The contour map for $\nabla^2\rho_{NEW}$ is similar to the AE case, but the local charge concentration ($\nabla^2\rho < 0$) present at Br is absent. Instead, a local charge depletion ($\nabla^2\rho > 0$) is found. Better agreement is obtained between the contour maps of $\nabla^2\rho_{AE}$ and $\nabla^2\rho_{ORT}$. When orthogonalized core orbitals are used a local charge concentration on both sides of the Br atom arise. Qualitatively, the $\nabla^2\rho_{AE}$ and $\nabla^2\rho_{ORT}$ contour maps are equal.

**TABLE III.**
**Properties of Electron Density Critical Points in Bromine and Sulfur Compounds.**

| Molecule A—B Bond | Method | $\rho(\mathbf{r}_c)$ ($e \cdot au^{-3}$) | $\nabla^2\rho(\mathbf{r}_c)$ ($e \cdot au^{-5}$) | $H(\mathbf{r}_c)$ (hartree $\cdot$ $au^{-3}$) | $\varepsilon$ | $\mathbf{R}_{A\text{-}CP}$ (au) | Net Charge on **A** | Bond Order | $K(\mathbf{A})/K(\mathbf{A})_{AE}$ |
|---|---|---|---|---|---|---|---|---|---|
| BrCl | | | | | | | | | |
| Br—Cl | AE | 0.125 | −0.039 | −0.059 | 0 | 1.950 | 0.153 | 1.309 | 1.000 |
| Br—Cl | NEW | 0.122 | −0.002 | −0.052 | 0 | 1.932 | 0.195 | 1.321 | 0.994 |
| Br—Cl | ECP | 0.121 | −0.040 | −0.057 | 0 | 1.908 | 0.203 | 1.314 | — |
| Br—Cl | ORT | 0.127 | −0.022 | −0.061 | 0 | 1.913 | 0.206 | 1.329 | 0.998 |
| BrI | | | | | | | | | |
| Br—I | AE | 0.0865 | 0.011 | −0.033 | 0 | 2.456 | −0.232 | 1.295 | 1.000 |
| Br—I | NEW | 0.0849 | 0.017 | −0.034 | 0 | 2.405 | −0.204 | 1.306 | 0.994 |
| Br—I | ECP | 0.0819 | −0.040 | −0.026 | 0 | 2.534 | −0.241 | 1.290 | — |
| Br—I | ORT | 0.0874 | 0.011 | −0.035 | 0 | 2.446 | −0.231 | 1.305 | 0.998 |
| LiBr | | | | | | | | | |
| Br—Li | AE | 0.036 | 0.220 | +0.004 | 0 | 2.788 | −0.938 | 0.153 | 1.000 |
| Br—Li | NEW | 0.036 | 0.218 | +0.003 | 0 | 2.790 | −0.938 | 0.154 | 0.994 |
| Br—Li | ECP | 0.036 | 0.218 | +0.003 | 0 | 2.790 | −0.938 | 0.154 | — |
| Br—Li | ORT | 0.037 | 0.227 | +0.003 | 0 | 2.797 | −0.936 | 0.157 | 0.998 |
| $H_2S$ | | | | | | | | | |
| S—H | AE | 0.215 | −0.628 | −0.198 | 0.104 | 1.624 | −0.027 | 1.080 | 1.000 |
| S—H | NEW | 0.214 | −0.578 | −0.188 | 0.109 | 1.604 | −0.039 | 1.081 | 0.979 |
| S—H | ECP | 0.214 | −0.619 | −0.196 | 0.121 | 1.582 | 0.216 | 1.081 | — |
| S—H | ORT | 0.212 | 0.112 | −0.282 | 0.499 | 1.153 | 0.916 | 1.101 | 0.993 |
| $SF_6$ | | | | | | | | | |
| S—F | AE | 0.223 | 0.507 | −0.245 | 0.000 | 1.134 | 4.268 | 0.490 | 1.000 |
| S—F | NEW | 0.228 | 0.462 | −0.211 | 0.002 | 1.158 | 4.167 | 0.530 | 0.983 |
| S—F | ECP | No (3, −1) bond critical point found | | | | | | | |
| S—F | ORT | 0.210 | 1.052 | −0.206 | 0.002 | 1.100 | 4.758 | 0.380 | 0.993 |

The topological analysis of the density obtained using ECPs on third-row atoms does not fail in all cases. In $H_2S$ for example, even when an ECP is used for the sulfur atom, a (3, −1) critical point between S and H atoms exists. There are also two (3, −3) critical points located at 1.372 au from the S atom in the direction of the H atoms. The coordinates of the (3, −1) critical point and all topological properties are almost identical to the AE results (see Table III). The values resulting from $\rho_{NEW}$ are reasonable, but the use of the orthogonalized core yields worse results for $H(\mathbf{r}_c)$ and $\varepsilon$, and it gives a wrong value for the Laplacian. On the other hand, $\rho_{NEW}$ and $\rho_{ORT}$ do not exhibit spurious (3, −3) critical points.

The correct behavior of $\rho_{ECP}$ for some cases does not guarantee that it will work properly in all cases. In $SF_6$ the same pseudopotential was used at the sulfur atom as in $H_2S$. However, no (3, −1) bond critical points could be found between sulfur and fluorine.

The addition of the core density causes an increase in the $\nabla^2\rho(\mathbf{r}_c)$ value and, in some cases, results in displacement of the bond critical point and can lead to overestimated net charges (Tables II, III). The increase of the Laplacian is due to the fact that the core electron density yields a positive contribution to the total Laplacian of the electron density at the bond critical point, because the core electrons are concentrated within a relatively small area about the nuclear center and depleted outside of this area.

For the homonuclear diatomic molecules reported in Table IV, $\rho_{ECP}$ provides a good approximation to the AE density at the (3, −1) critical point. The difference between $\rho_{ECP}$ and $\rho_{AE}$ seems to be within the error resulting from the application of different basis sets. The Laplacian of $\rho_{ECP}(\mathbf{r}_c)$ is also in reasonable agreement with $\nabla^2\rho_{AE}(\mathbf{r}_c)$, although the error is somewhat larger than for $\rho_{ECP}$ itself. The electronic energy density, $H(\mathbf{r}_c)$, obtained from the ECP density matrix is

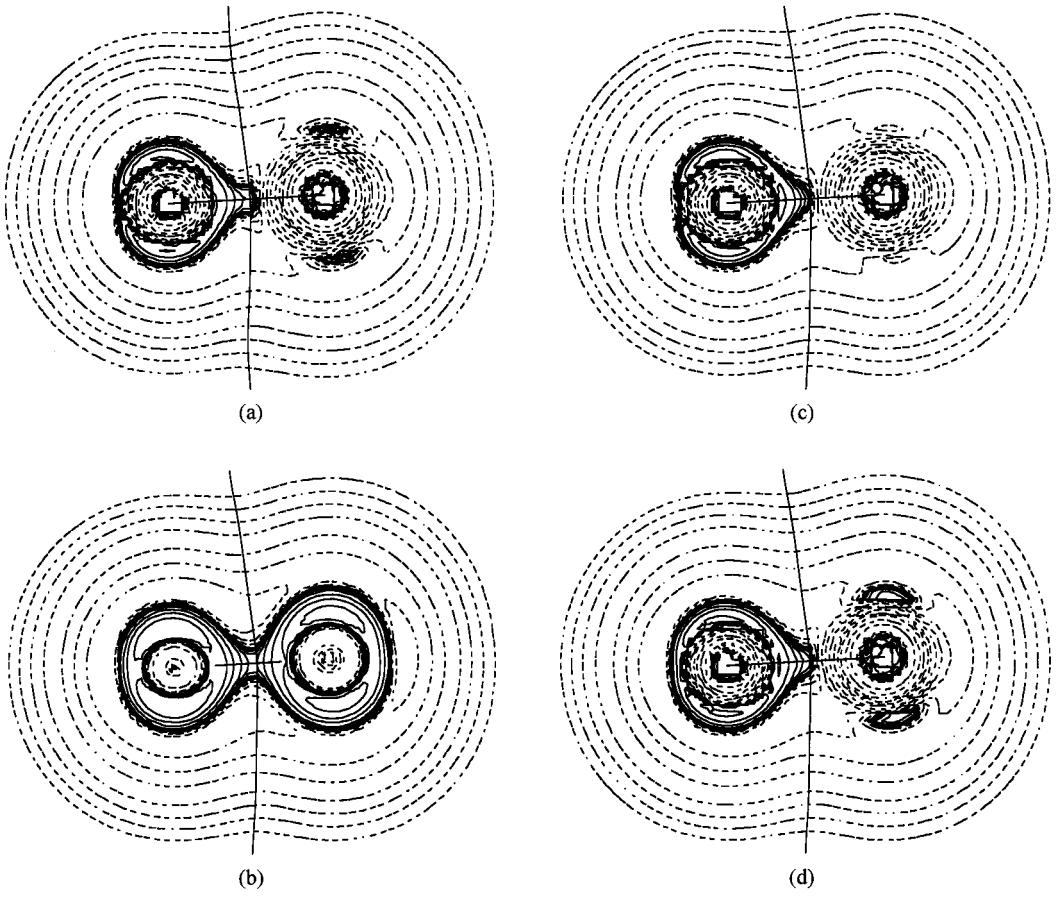


**FIGURE 4.** Contour maps of the Laplacian of the electron density $\nabla^2\rho$ in BrCl. (—) $\nabla^2\rho < 0$ and (- - -) $\nabla^2\rho > 0$. The lines correspond to $\nabla^2\rho$ values of $\pm 1 \cdot 10^{-3}$, $\pm 2 \cdot 10^{-n}$, $\pm 4 \cdot 10^{-n}$, $\pm 8 \cdot 10^{-n}$, $n$ running from $-3$ to $+2$. (a) All-electron density $\rho_{AE}$, (b) density obtained from the pseudopotential calculation $\rho_{ECP}$, (c) density obtained by addition of core density to pseudopotential density $\rho_{NEW}$, (d) density obtained by addition of orthogonalized core density to pseudopotential density $\rho_{ORT}$. The chlorine atom is shown at the left side; the bromine atom is at the right side.

also in good accordance with the AE value. The density $\rho_{NEW}$ exhibits an improvement over $\rho_{ECP}$. The values of $\rho_{ECP}(\mathbf{r}_c)$ and $\rho_{NEW}(\mathbf{r}_c)$ are practically identical, but $\nabla^2\rho_{NEW}(\mathbf{r}_c)$ fails for $I_2$ and $As_2$, giving the wrong sign for both molecules. The orthogonalization of core orbitals slightly improves the results. $\rho_{ORT}(\mathbf{r}_c)$ and $H(\mathbf{r}_c)$ are slightly better, and $\nabla^2\rho_{ORT}(\mathbf{r}_c)$ has a negative sign as in the AE case. The bond order differs little among the four approaches. Both ECP and ECP with added core densities slightly overestimates the bond order in comparison with the AE values.

The diphosphorus molecule presents an interesting special case. For all four electron densities studied here, there is no $(3, -1)$ critical point between the phosphorus atoms but rather a local maximum, i.e., a $(3, -3)$ critical point. Such maxima and corresponding pseudoatoms were observed before for other molecules. In some cases, the maxima disappear at a higher level of theory,[25] but sometimes they persist even though correlated wave function and large basis sets are employed.[5] Between the nucleus and the nonnuclear maximum is a $(3, -1)$ critical point, except for $\rho_{ECP}$. Such nonnuclear electron density maxima make it possible to calculate atomic properties only if the integration is performed over the pseudoatom as well. In so doing, the results cannot be immediately compared with those obtained for a system without nonnuclear maxima. Thus, we only compare the properties of the electronic density at this maximum. The simple addition of core density does not improve the Laplacian of the electron density or $H(\mathbf{r}_c)$, but the properties calculated from $\rho_{ORT}$ agree with those of $\rho_{AE}$.

Transition metal complexes are probably the main area of application of ECP. As shown in Table V, the topological analysis of the electron

**TABLE IV.**
**Properties of Electron Density Critical Points in Some Diatomic Molecules.**

| Molecule A—B Bond | Method | $\rho(\mathbf{r}_c)$ ($e \cdot au^{-3}$) | $\nabla^2\rho(\mathbf{r}_c)$ ($e \cdot au^{-5}$) | $H(\mathbf{r}_c)$, (hartree $\cdot$ $au^{-3}$) | $\mathbf{R}_{A\text{-}CP}$ (au) | Bond Order | $K(\mathbf{A}) / K(\mathbf{A})_{AE}$ |
|---|---|---|---|---|---|---|---|
| $Cl_2$ | | | | | | | |
| Cl—Cl | AE | 0.152 | −0.069 | −0.076 | 1.902 | 1.316 | 1.000 |
| Cl—Cl | NEW | 0.151 | −0.078 | −0.081 | 1.902 | 1.349 | 0.973 |
| Cl—Cl | ECP | 0.151 | −0.081 | −0.081 | 1.902 | 1.347 | — |
| Cl—Cl | ORT | 0.158 | −0.092 | −0.087 | 1.902 | 1.364 | 0.992 |
| $Br_2$ | | | | | | | |
| Br—Br | AE | 0.104 | −0.034 | −0.043 | 2.190 | 1.318 | 1.000 |
| Br—Br | NEW | 0.102 | −0.019 | −0.039 | 2.190 | 1.327 | 0.994 |
| Br—Br | ECP | 0.101 | −0.028 | −0.040 | 2.190 | 1.322 | — |
| Br—Br | ORT | 0.106 | −0.030 | −0.044 | 2.190 | 1.335 | 0.998 |
| $I_2$ | | | | | | | |
| I—I | AE | 0.074 | −0.015 | −0.026 | 2.548 | 1.336 | 1.000 |
| I—I | NEW | 0.070 | 0.003 | −0.022 | 2.548 | 1.328 | 0.998 |
| I—I | ECP | 0.069 | −0.026 | −0.024 | 2.548 | 1.321 | — |
| I—I | ORT | 0.073 | −0.009 | −0.026 | 2.548 | 1.335 | 0.999 |
| $As_2$ | | | | | | | |
| As—As | AE | 0.128 | −0.058 | −0.075 | 1.989 | 3.045 | 1.000 |
| As—As | NEW | 0.121 | 0.020 | −0.058 | 1.989 | 3.050 | 0.996 |
| As—As | ECP | 0.115 | −0.128 | −0.065 | 1.989 | 3.038 | — |
| As—As | ORT | 0.122 | −0.016 | −0.0682 | 1.989 | 3.041 | 0.999 |
| $P_2$ | | | | | | | |
| P—P | AE | 0.189 | −0.402 | −0.173 | 1.773 | | |
| P—P | NEW | 0.171 | −0.317 | −0.148 | 1.773 | Maximum of $\rho(\mathbf{r}_c)$ in the center | |
| P—P | ECP | 0.170 | −0.354 | −0.152 | 1.773 | | |
| P—P | ORT | 0.177 | −0.406 | −0.172 | 1.773 | | |

density using an ECP in $(CO)_5Mo(CH_2)$ is successful if the small-core (SC) pseudopotential density $\rho_{SC\text{-}ECP}$ is used. The calculated properties are nearly identical with the AE values, and the addition of core density does not influence the results significantly. This is due to the fact that the inner-core orbitals lie very close to the nucleus. The inner-core density has a very low magnitude in the chemically interesting area. The orthogonalization of core orbitals has little effect on the topology of $\rho_{SC\text{-}ECP}$ for the $(CO)_5Mo(CH_2)$ complex. The exclusion of the outer-core $5s$ and $5p$ electrons from the calculation has a dramatic effect upon the results of the topological analysis. this becomes obvious by the results obtained using the large-core (LC) ECP density, $\rho_{LC\text{-}ECP}$, which differs strongly from the SC data. Only one bond critical point between Mo and one of the carbon atoms was found, and its properties do not agree with the AE or with the SC-ECP results. For the Mo—$CH_2$ and the Mo—$CO_{trans}$ bonds, all attempts to find $(3, -1)$ critical points failed. The addition of molybdenum core orbitals to the LC density brings a significant improvement. All bond critical points were found to have comparable properties with those using the AE density, although the accuracy of the results is clearly lower than in the SC-ECP approach. The orthogonalization process works well for LC-ECP cases, and the numerical results for the topological properties of $\rho_{LC\text{-}ORT}$ agree well with the values obtained for $\rho_{SC\text{-}ECP}$.

For titanium tetrafluoride (Table VI), the values of $\rho_{AE}(\mathbf{r}_c)$ and $\nabla^2\rho_{AE}(\mathbf{r}_c)$ are well reproduced by SC $\rho_{ECP}(\mathbf{r}_c)$, but $-H(\mathbf{r}_c)$ is strongly underestimated. This result does not change significantly by using $\rho_{NEW}$ or $\rho_{ORT}$, although the latter provides a slightly better estimation for the density but not for the Laplacian. Unlike $(CO)_5Mo(CH_2)$, the topological analysis of LC-ECP density does not fail completely. However, the calculated properties of

**TABLE V.**
**Properties of Electron Density Critical Points in $(CO)_5Mo(CH_2)$.**

| A—B Bond | Method | $\rho(\mathbf{r}_c)$ $(e \cdot au^{-3})$ | $\nabla^2\rho(\mathbf{r}_c)$ $(e \cdot au^{-5})$ | $H(\mathbf{r}_c)$, (hartree · $au^{-3}$) | $\varepsilon$ | $\mathbf{R}_{A\text{-}CP}$ (au) |
|---|---|---|---|---|---|---|
| Mo—$CH_2$ | SC-NEW | 0.122 | 0.437 | −0.042 | 0.023 | 1.948 |
| Mo—$CH_2$ | SC-ECP | 0.122 | 0.437 | −0.042 | 0.022 | 1.947 |
| Mo—$CH_2$ | SC-ORT | 0.124 | 0.460 | −0.041 | 0.031 | 1.965 |
| Mo—$CH_2$ | LC-NEW | 0.135 | 0.336 | −0.038 | 0.069 | 2.012 |
| Mo—$CH_2$ | LC-ECP | No (3, −1) bond critical point found | | | | |
| Mo—$CH_2$ | LC-ORT | 0.119 | 0.464 | −0.038 | 0.034 | 1.970 |
| Mo—CO *cis* | SC-NEW | 0.088 | 0.481 | −0.013 | 0.137 | 2.011 |
| Mo—CO *cis* | SC-ECP | 0.088 | 0.481 | −0.013 | 0.138 | 2.011 |
| Mo—CO *cis* | SC-ORT | 0.090 | 0.499 | −0.013 | 0.132 | 2.029 |
| Mo—CO *cis* | LC-NEW | 0.096 | 0.420 | −0.012 | 0.079 | 2.044 |
| Mo—CO *cis* | LC-ECP | 0.063 | 0.157 | −0.028 | 2.805 | 1.949 |
| Mo—CO *cis* | LC-ORT | 0.086 | 0.493 | −0.013 | 0.127 | 2.033 |
| Mo—CO *trans* | SC-NEW | 0.071 | 0.392 | −0.006 | 1.332 | 2.098 |
| Mo—CO *trans* | SC-ECP | 0.071 | 0.392 | −0.006 | 1.335 | 2.098 |
| Mo—CO *trans* | SC-ORT | 0.073 | 0.406 | −0.006 | 1.185 | 2.115 |
| Mo—CO *trans* | LC-NEW | 0.076 | 0.354 | −0.005 | 0.906 | 2.119 |
| Mo—CO *trans* | LC-ECP | No (3, −1) bond critical point found | | | | |
| Mo—CO *trans* | LC-ORT | 0.0700 | 0.403 | −0.007 | 1.268 | 2.117 |

LC, large core; SC, small core

the (3, −1) critical points disagree significantly with those obtained from the AE or SC-ECP calculations. As in the case of the Mo complex, better values are obtained using $\rho_{LC\text{-}ORT}$.

## Conclusions

The main drawback of using electron densities from ECP calculations, $\rho_{ECP}(\mathbf{r})$, in the topological analysis is the absence of bond critical points. This can be corrected by adding atomic core electron densities. The simple addition of core-electron density to $\rho_{ECP}(\mathbf{r})$ is sufficient to reproduce a qualitatively correct topology of the electron density at the bond critical points. We studied two different schemes for the core density. In the first one, $\rho_{ECP}(\mathbf{r})$, atomic core-electron density obtained from a single-atom restricted Hartree–Fock calculation is added to $\rho_{ECP}(\mathbf{r})$. In the second scheme, all the core orbitals are orthogonalized to the valence molecular orbitals using the Gram–Schmidt orthogonalization procedure, keeping the valence orbitals' original shape.

**TABLE VI.**
**Properties of Electron Density Critical points of Ti—F Bond in $TiF_4$.**

| A—B Bond | Method | $\rho(\mathbf{r}_c)$ $(e \cdot au^{-3})$ | $\nabla^2\rho(\mathbf{r}_c)$ $(e \cdot au^{-5})$ | $H(\mathbf{r}_c)$, (hartree · $au^{-3}$) | $\mathbf{R}_{A\text{-}CP}$ (au) |
|---|---|---|---|---|---|
| Ti—F | LC-NEW | 0.1727 | 0.8951 | −0.0074 | 1.691 |
| Ti—F | LC-ECP | 0.0922 | −0.1761 | −0.1136 | 1.297 |
| Ti—F | LC-ORT | 0.1526 | 1.0286 | −0.0107 | 1.673 |
| Ti—F | SC-NEW | 0.1519 | 1.0804 | −0.0070 | 1.650 |
| Ti—F | SC-ECP | 0.1519 | 1.0803 | −0.0070 | 1.650 |
| Ti—F | SC-ORT | 0.1549 | 1.1242 | −0.0065 | 1.660 |

For all methods the ellipticity value is zero.

Our results show that the first scheme is able to reproduce local properties such as $\rho(\mathbf{r}_c)$, $\nabla^2\rho(\mathbf{r}_c)$, $H(\mathbf{r}_c)$, etc., as well as global properties (bond orders, atomic kinetic energies, or atomic net charges) in a reasonable way.

In the second scheme using orthogonal orbitals, a good agreement between the values of the atomic kinetic energy $K(\mathbf{A})$ and the AE $K(\mathbf{A})_{AE}$ was obtained. This was not the case for the bond orders or the net charges, where high positive charge and low bond orders were found. Local properties, especially $\nabla^2\rho_{ORT}(\mathbf{r}_c)$, show quite different values from those calculated using $\rho_{AE}$ or $\rho_{NEW}$. In some cases, positive values were incorrectly obtained for $\nabla^2\rho_{ORT}(\mathbf{r}_c)$. The Gram–Schmidt orthogonalization procedure used here does not provide an improvement over $\rho_{NEW}$.

For transition metals, the electron density obtained from a SC-ECP calculation is good enough to reproduce not only the correct topology of the metal–ligand bonds but the values of the local properties as well. It is not necessary to add the metal's core density because the deeper metal core has little impact on the topological properties of $\rho_{SC\text{-}ECP}$. On the other hand, the LC-ECP approach produces densities that give wrong topologies.

## Acknowledgments

We wish to express our gratitude to Dr. S. Grimme (Universität Bonn) for a stimulating discussion and A. Lupinetti for critically reading the manuscript. The work was supported by the Fonds der Chemischen Industrie and by the Deutsche Forschungsgemeinschaft (SFB 260). S.F.V. thanks the Deutscher Akademischer Austauschdienst for a scholarship. The computer time was provided by the Universitätsrechenzentrum Giessen.

## References

1. G. Frenking, I. Antes, M. Böhme, S. Dapprich, A. W. Ehlers, V. Jonas, A. Neuhaus, M. Otto, R. Stegmann, A. Veldkamp, and S. F. Vyboishchikov, In *Reviews in Computational Chemistry*, Vol. 8, D. B. Boyd and K. B. Lipkowitz, Eds. VCH Publishers, New York, 1996, p. 63.
2. P. Pyykkö, *Chem. Rev.*, **88,** 563 (1988).
3. (a) V. Bonifacic and S. Huzinaga, *J. Chem. Phys.*, **65,** 2322 (1976), **64,** 956 (1976); (b) Y. Sakai, E. Miyoshi, M. Klobukowski, and S. Huzinaga, *J. Comput. Chem.*, **8**, 256 (1987); (c) L. Seijo, Z. Barandiaran, and S. Huzinaga, *J. Chem. Phys.*, **93,** 5843 (1990).
4. R. F. W. Bader, *Atoms in Molecules*: *A Quantum Theory*, Clarendon Press, Oxford, UK, 1990.
5. W. L. Cao, C. Gatti, P. J. MacDougall, and R. F. W. Bader, *Chem. Phys. Lett.*, **141,** 380 (1987).
6. (a) R. F. W. Bader and H. Essén, *J. Chem. Phys.*, **80,** 1943 (1984); (b) R. F. W. Bader, P. J. MacDougall, and C. D. H. Lau, *J. Am. Chem. Soc.*, **106,** 1594 (1984).
7. D. Cremer and E. Kraka, *Angew. Chem.*, **96,** 612 (1984), *Angew. Chem. Int. Ed. Eng.*, **23,** 62 (1984), *Croat. Chem. Acta*, **57,** 1259 (1984).
8. (a) C. Bo, J. M. Poblet, and M. Bénard, *Chem. Phys. Lett.*, **141,** 380 (1990); (b) Z. Lin and M. B. Hall, *Inorg. Chem.*, **31,** 2791 (1992); (c) R. Stegmann, A. Neuhaus, and G. Frenking, *J. Am. Chem. Soc.*, **115,** 11930 (1993); (d) A. Neuhaus, A. Veldkamp, and G. Frenking, *Inorg. Chem.*, **33,** 5278 (1994); (e) M. Böhme, G. Frenking, and M. T. Reetz, *Organometallics*, **13,** 4237 (1994).
9. A. Sierraalta and F. Ruete, *J. Comput. Chem.* **15,** 313 (1994).
10. C. Bo, M. Costas, and J. M. Poblet, *J. Phys. Chem.*, **99,** 5914 (1995).
11. (a) A. Bergner, M. Dolg, W. Küchle, H. Stoll, and H. Preuss, *Mol. Phys.*, **80,** 1431 (1993); (b) H. Stoll, P. Fuentealba, P. Schwerdtfeger, J. Flad, L. v. Szentpály, and H. Preuss, *J. Chem. Phys.*, **81,** 2732 (1984).
12. P. J. Hay and W. R. Wadt, *J. Chem. Phys.*, **82,** 299 (1985).
13. V. Jonas, G. Frenking, and M. T. Reetz, *J. Comput. Chem.*, **13,** 919 (1992).
14. P. J. Hay and W. R. Wadt, *J. Chem. Phys.*, **82,** 270 (1985).
15. R. Krishnan, J. Binkley, R. Seeger, and J. A. Pople, *J. Chem. Phys.*, **72,** 650 (1980).
16. A. D. MacLean and G. S. Chandler, *J. Chem. Phys.*, **72,** 5639 (1980).
17. J. Andzelm, S. Huzinaga, M. Klobukowski, E. Radzio, Y. Sakai, and H. Tatewaki, Gaussian Basis Sets for Molecular Calculations, Elsevier, Amsterdam, 1984.
18. M. J. Frisch, G. W. Trucks, M. Head–Gordon, P. M. W. Gill, M. W. Wong, J. B. Foresman, B. G. Johnson, H. B. Schlegel, M. A. Robb, E. S. Replogle, R. Gomperts, J. L. Andres, K. Raghavachari, J. S. Binkley, C. Gonzalez, R. L. Martin, D. J. Fox, D. J. Defrees, J. Baker, J. J. P. Stewart, and J. A. Pople, *Gaussian 92, Revision G.3*, Gaussian, Inc., Pittsburgh, PA, 1992.
19. F. W. Biegler–König, R. F. W. Bader, and T.-H. Tang, *J. Comput. Chem.*, **3,** 317 (1982).
20. R. F. W. Bader, *J. Chem. Phys.*, **73,** 2870 (1980).
21. F. W. Biegler–König and A. J. Duke, *PROAIM Program*, McMaster University, Hamilton, Canada, 1983.
22. J. Ángyán, M. Loos, and I. Mayer, *J. Phys. Chem.*, **98,** 5244 (1994).
23. J. Cioslowski and S. T. Mixon, *J. Am. Chem. Soc.*, **113,** 4142 (1991).
24. R. F. W. Bader, T. S. Slee, D. Cremer, and E. Kraka, *J. Am. Chem. Soc.*, **105,** 5069 (1983).
25. C. Gatti, P. J. MacDougall, and R. F. W. Bader, *J. Chem. Phys.*, **88,** 3792 (1988).